4.22   ROLE OF THE SHEAR AND INVERSION STRENGTH DURING SUNSET TURBULENCE
OVER LAND: CHARACTERISTIC LENGTH SCALES

David Pino [*]
Applied Physics Department, Technical University of Catalonia, and
Institute for Space Studies of Catalonia (IEEC/CSIC), Barcelona, Spain
Harm J. J. Jonker
Thermal and Fluids Sciences Section, Department of Multi-Scale Physics, Delft University of Technology, Delft,
The Netherlands
Jordi Vilà-Guerau de Arellano and Alessandro Dosio
Meteorology and Air Quality Section, Wageningen University, Wageningen, The Netherlands

1. INTRODUCTION

Near sunset, the surface heat flux progressively decreases, consequently the convective eddies which maintain turbulence start to loose their strength and the convective turbulence in the boundary layer begins to decay. Several authors have previously studied this transition regime of atmospheric turbulence. Experimentally Monin and Yaglom (1975) studied the decay of grid-generated turbulence under neutral unconfined conditions. During the decay, the turbulence maintains the initial isotropy. The energy decay follows a power law $(t - t_0)^n$. Stillinger et al. (1983) studied the decay of homogeneous turbulence in a uniform stratification showing that turbulence becomes highly anisotropic. On the other hand, turbulence decay has been studied by using theoretical models (Goulart et al., 2003) or numerical simulations (Nieuwstadt and Brost, 1986; Sorbjan, 1997; Goulart et al., 2003). All these studies used Large Eddy Simulation (LES) models to describe some of the characteristics of the boundary layer during turbulence decay. Recently, Shaw and Barnard (2002) used Direct Numerical Simulation to study the same problem. Moreover, Caughey and Kaimal (1977), Grant (1997), Grimsdell and Angevine (2002) and Anfossi et al. (2004) reported some observations and in some cases compared it with LES results.

In this study, by analyzing LES results, the role played by the inversion strength and shear during the decay of convective turbulence is discussed. Particular effort is done in describing the evolution of the characteristic length scales during this process. This study is inspired by the work of Nieuwstadt and Brost (1986) (hereafter NB86). By using LES, they analyzed an idealized case of the decay of turbulence of several dry convective boundary layers with constant geostrophic wind (5 m s^{-1}) and different $\Delta\theta$, $\overline{\theta}$ and boundary layer height. Time evolution of the volume averaged variables, vertical profiles and convection patterns are compared in order to determine which processes are relevant during the decay. For one of their cases, they found a different behavior in the decay of turbulence characterized by the return

Corresponding author address: David Pino, Applied Physics Department, Technical University of Catalonia, Av del Canal Olímpic s/n, 08860 Castelldefels, Spain; e-mail: david@fa.upc.es.

to equilibrium levels of warm air parcels, *i.e.*, 'demixing' process. Recently, Grimsdell and Angevine (2002) relate wind profiler observations of the boundary layer during the afternoon transition to the turbulence decay process described by NB86.

In our study, apart from studying the evolution of different atmospheric variables during the decay of turbulence, we focus on the evolution of characteristic length scale during the decay of a dry convective boundary layer. This aspect has not been intensively studied by previous works, except by Grant (1997) who calculated the spectra of the vertical velocity at different times and height during an observational campaign during August 1990. He found that in the boundary layer the spectral peak moves to smaller wavelengths. By using LES, NB86 and Goulart et al. (2003) found that the position of the peak remains constant during their simulations. Conversely, Sorbjan (1997) showed that the spectral peak shifts towards larger eddies, *i.e.*, the larger eddies decay slower than the smaller ones. Therefore, an important aspect of this study is to clarify the evolution of the characteristic length scale during the decay of turbulence.

2. NUMERICAL SETUP

Four different runs of the LES model described in Cuijpers and Duynkerke (1993) and recently modified by Cuijpers and Holtslag (1998) were done. Different wind profiles and inversion strengths are prescribed. Each decay experiment begins with a fully developed dry convective boundary layer, which has been generated by heating the surface during two hours at a constant rate ($\overline{w\theta}_0 = 0.1$ K m s^{-1}, $\overline{wq}_0 = 0$). At this moment (t_0) the surface heat flux is set to zero, two hours more were simulated, and the statistics were calculated every two minutes. The simulated domains were $12.8 \times 12.8 \times 2.048$ km^3 with grid spacing $\Delta x = \Delta y = 50$ m and $\Delta z = 16$ m.

The differences between the four runs are basically based on the inversion strengths and mean winds derived at $t = t_0 - 2$ hours. Regarding the shear cases, a pure buoyancy driven boundary layer, without geostrophic winds, namely NS (no shear), and a boundary layer driven both by buoyancy and shear (GC, geostrophic constant), where the geostrophic wind is constant with height ($U_g = 10$ m s^{-1}, $V_g = 0$ m s^{-1}) at the beginning of the

simulation, were considered. Regarding the temperature jump at the inversion, figure 1 shows the initial vertical profiles of the potential temperature for the two considered inversion strengths.
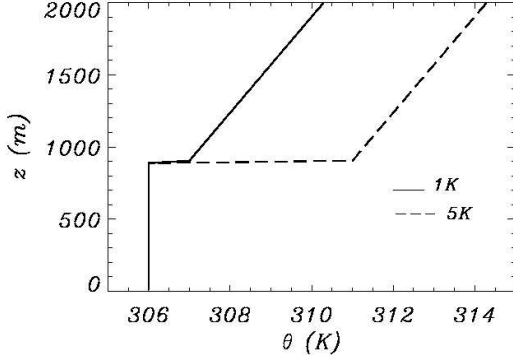

FIGURE 1: Initial vertical profiles of the potential temperature prescribed in the simulations.

The characteristics of the convective boundary layer just before the decay process starts (t_0) for each simulated case are presented in Table 1. In this table, h is the height where virtual potential temperature gradient is maximum, z_i is the height of the minimum buoyancy flux, $\Delta\theta = \theta(h) - \overline{\theta}$, $\Delta U = U(h) - \overline{U}$, where $\overline{\theta}$ and $\overline{U}$ are, respectively, the values of the potential temperature and horizontal velocity in the x direction in the boundary layer, and the Richardson number is defined as (Pino et al., 2003):

$$Ri = \frac{gh}{\overline{\theta}}\frac{\Delta\theta}{w_m^2}, \quad w_m^3 = w_*^3 + 8u_*^3 \qquad (1)$$

	NS1	NS5	GC1	GC5
$\overline{\theta}$ (K)	307.1	307.6	307.1	307.7
h (m)	1160	952	1044	936
z_i (m)	1072	896	1040	896
$\Delta\theta$ (K)	0.68	2.69	0.68	2.18
w_* (m s^{-1})	1.54	1.44	1.54	1.44
u_* (m s^{-1})	10^{-4}	10^{-4}	0.44	0.44
ΔU (m s^{-1})	0.031	0.014	1.01	1.03
Ri	10.6	39	9.4	27

Table 1: Boundary layer variables and scaling parameters at the beginning of the decay process for each simulation.

3. RESULTS

Following NB86, who showed that decay of turbulence is self-similar with respect the dimensionless time $t/t_* = tw_m h^{-1}$, we have used h/w_m and w_m^2 to nondimensionalize time and velocity variances respectively. By doing this, as the values for w_m and h presented in table 1 vary for each case, it is clear that different $tw_m h^{-1}$ are obtained for each case at the same time t.

3.1 *TKE and variances time evolution*

Figure 2 shows the turbulent kinetic energy (TKE) averaged over the boundary layer and normalized by means of w_m^2 as a function of $tw_m h^{-1}$. As shown, for all the studied cases, the TKE remains constant and the curves collapse onto a single curve during one eddy turnover time. After $tw_m h^{-1} \approx 1$, similarity is not fulfilled and NS and GC cases present different decay evolution, decaying faster the NS simulations. The exponent of the power law for the NS case at the beginning of the decay is similar to the unique exponent that NB86 found ($n = -1.2$) in all of their shear simulations. The shear cases present exponents which are similar to the to simulation D-1 of Sorbjan (1997). In his work, he did not suddenly shut-off surface heat flux, but decreased it with time. For 3D isotropic turbulence, Chasnov (1994) pointed that the exponent of the decay process is always lower than -1.
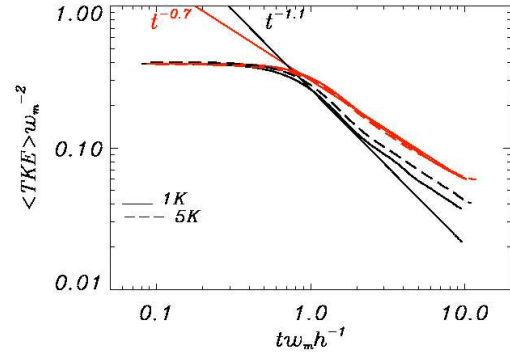

FIGURE 2: TKE averaged across the boundary layer and nondimensionalized by w_m^2 as a function of $tw_m h^{-1}$ for the NS (black) and GC simulations (red). The lines serve as a guide to the eye to give an indication of the decay rates.

If the horizontal components of the TKE are considered (not shown here), a vertical shift appears for $0.5 < u^2 >$ and the curves do not collapse for $tw_m h^{-1} < 1$. This fact is due to the different contribution of shear of the simulations. The decay of this component can be described by a power law with exponent $n \approx -1$ only for the NS cases, GC cases decay slowly. NB86 found an exponent of $n = -1$. The other horizontal component $(0.5 < v^2 >)$ presents approximately the same decay profile for all the cases. The vertical component, $0.5 < w^2 >$, collapse onto a single curve for $tw_m h^{-1} < 1$, but only the decay process for NS can be approximately reproduced by a power law with exponent -2. For the GC cases, the exponent is larger and seems to change with time. These facts can be understood as follows. For a decay process with a confined outer length scale, like w bounded by h, a power law with an exponent $n \sim -2$ is expected (e.g. NB86). However, the length scales of u and v, which are confined by the domain size, can grow unbounded for quite a while, implying an exponent $n > -2$. Therefore, the anisotropy must increase. In order to summarize these characteristics and to verify this last point, figure 3

shows the time evolution of an anisotropy variable defined as $(<u^2> + <v^2>)(2<w^2>)^{-1}$. Clear differences between shear and no shear cases can be observed at the beginning of the decay. The shear cases present an almost perfect isotropy. On the contrary, NS cases are much more anisotropic in the vertical direction, specially NS1. For $tw_m h^{-1} \gtrsim 1$, anisotropy grows for all the cases. However, the growth rate depends on time: the exponent of the power laws which reproduce the decay process are not constant. For one of the cases (NS1), the horizontal profile of the anisotropy for $2 < tw_m h^{-1} < 3.5$ is related with a large increase of $<w^2>$ which was also found by NB86 for one of their simulations. As we will show this increase is related with some special features during the decay process. The shear cases have a tendency to an asymptotic value after $tw_m h^{-1} = 3$. In all the cases, turbulence does not relax to an isotropic state. A first analysis of the instantaneous horizontal cross sections at the bulk shows that the 3D-turbulence structures of the boundary layer become with the characteristics of 2D-turbulence for the NS cases. Further analysis is needed to verify this point.

The variance of temperature averaged across the boundary layer (not shown here) starts to decay almost immediately and all the cases reveal a different time evolution. This can be due to the fact that temperature variance is dominated by near surface production.
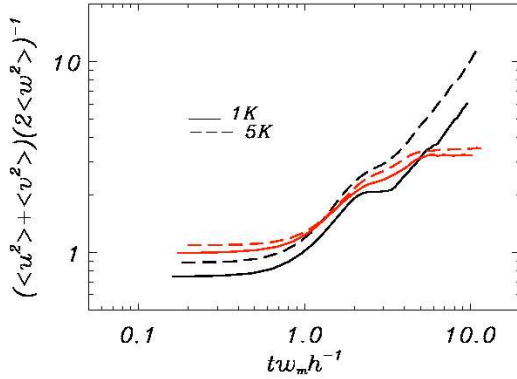

FIGURE 3: Anisotropy as a function of $tw_m h^{-1}$ for the NS (black) and GC simulations (red).

3.2 *Vertical profiles of potential temperature and buoyancy flux*

No differences in the evolution of potential temperature vertical profile (not shown here) are found between shear and no shear cases. For all the studied cases, shortly after the beginning of the decay ($t = 14$ minutes, $tw_m h^{-1}$ around 1.3) a positive gradient of the potential temperature can be found throughout the boundary layer.

The vertical profile of the buoyancy flux gives us one of the keys to understand the decay process. The buoyancy flux evolution is as follows. At the beginning of the process, heat flux at the surface becomes zero but at higher levels it remains positive until $t \approx 18$ min-

utes ($tw_m h^{-1}$ around 1.6), which corresponds with the period when the averaged TKE in the boundary layer is constant and when a positive lapse rate appears in the boundary layer. Afterward, as entrainment takes place continuously, a negative heat flux profile is found in the whole boundary layer. Thereafter, all the cases show a reverse on the flux sign, and a positive buoyancy flux in the boundary layer for $30 \lesssim t \lesssim 50$ minutes. However, differences can be observed between the cases. NS5, which is the case with low entrainment rates due the the large inversion strength and no shear, presents the lowest values of the positive buoyancy flux. Figure 4 shows the buoyancy flux after 36 minutes. At this moment all cases show a positive flux in the middle of the boundary layer. NS5 has the lowest positive buoyancy flux. Afterward, the fluxes turn to negative and tend to zero except for NS1 which turns another time to positive for $66 < t < 80$ minutes. This sort of oscillating behavior was observed by Caughey and Kaimal (1977) and Grimsdell and Angevine (2002) and it is similar only to one of the numerical experiments of NB86. They named it 'demixing' and associated it to cycles in the conversion between kinetic and potential energy. In some cases, when there is not enough small scale turbulence in order to mix the big parcels of warm air coming from above the inversion, moving downward until they have expended all their energy. Then, they tend to return to their equilibrium levels, moving upward and producing a positive buoyancy flux in the middle of the boundary layer.
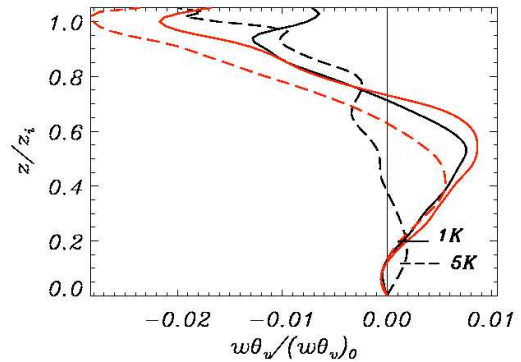

FIGURE 4: Buoyancy flux nondimensionalized by its surface value after 36 minutes for the NS cases (black) and GC cases (red). This time corresponds to $tw_m h^{-1} = 2.86, 3.24, 3.36$ and 3.54 for NS1, NS5, GC1 and GC5 respectively.

NB86 concluded that the appearance of demixing in a sheared convective boundary layer seems to depend on the strength of the inversion. Very large ΔT would prevent entrainment and consequently the production of temperature fluctuations. However, in their study they did not consider large ΔT and only found demixing effects for the experiment with the largest inversion strength ($\Delta T = 2$ K). Two important aspects should be noticed. First, it is not clear how exactly NB86 defined ΔT. If they used a similar definition, our inversion strengths were comparable. Second, in their simulations, other variables apart

from inversion strength should be considered to explain why there is no demixing for the experiments with the smallest inversion strength. In other words, in the experiments of NB86 many parameters vary (for instance, if the initial surface heat flux is the same for the different experiments, $\overline{T}$ can vary by 1.5 times between them), so it is difficult to extract the influence of inversion strength on demixing effects. In our numerical experiments, where we only vary $\Delta\theta$ and u_*, we find demixing effects for all the cases: NS1 and GC1 with small inversion strength, GC5 which corresponds to a large inversion strength with shear and also for NS5 with a large inversion and no shear. However it is clear that for this last case the demixing effects are not so important. A possible explanation to find out when demixing effects appear could be based in considering the role of the shear in the entrainment process. As it is already known shear enhances entrainment (Pino et al., 2003). In consequence, shear can contribute to favor demixing.

3.3 *Characteristic length scales*

In this section we focus on the spectra of u and w at $z/h \approx 0.5$. Figure 5 shows the vertical velocity spectra for NS1 obtained for $t = 2$, 42 and 80 minutes. As can be observed the spectral peak shift towards larger eddies at $t = 42$ minutes ($tw_m h^{-1} = 3.34$). At this moment NS1 presents a positive buoyancy flux in the middle of the boundary layer. For the last represented time, the peak returns to its original value. The same behavior was observed for NS5. Shortly, the spectral peak is shifted towards larger scales during demixing, returning to its original value afterward. Demixing can be associated to an increase of the characteristic length scale.
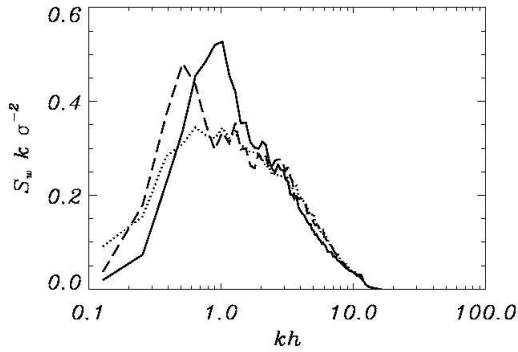

FIGURE 5: Spectral density normalized by σ^2/k, where σ^2 is the area below the spectral curve, calculated at $z/h \approx 0.5$ for $t = 2$ (solid), 42 (dashed), and 80 minutes (dotted) for NS1 ($tw_m h^{-1} = 0.16$, 3.34 and 4.8 respectively).

Figure 6 shows the time evolution of the spectral peak of the vertical velocity spectra (Λ_w) for the NS simulations. As can be observed both cases presents a similar evolution until $tw_m h^{-1} \approx 5$. During one eddy turnover time the characteristic length scale remains constant. After a small increase, Λ_w decrease below h for both cases

and remains constant during one eddy turnover time approximately. At this period a negative vertical profile of the buoyancy flux is found in the boundary layer. Afterward, the buoyancy flux turns to positive. This fact is related with an increase of Λ_w between $tw_m h^{-1} \approx 3$ and $tw_m h^{-1} \approx 5$. Once the flux becomes negative another time, Λ_w decreases for both cases. At $tw_m h^{-1} > 5$, NS5 presents a constant value of Λ_w, being $\Lambda_w < h$ until the end of the simulation. However, for NS1 the characteristic length scale increases its value when the buoyancy flux is positive another time. Notice that this is the only case that presents a positive buoyancy flux for $tw_m h^{-1} \gtrsim 5$.

The evolution of the spectral peak of the vertical velocity spectra for the shear cases is presented in figure 7. During one eddy turnover time the evolution is similar to the no shear cases. Once a negative buoyancy flux exists in the whole boundary layer, and the characteristic length scale has decreased its value for both cases, it remains constant even if a positive buoyancy flux exists after this moment. Shear seems to set the characteristic length scale of the vertical velocity spectra. Future research will be addressed to study the effects of shear on the characteristic length scale.
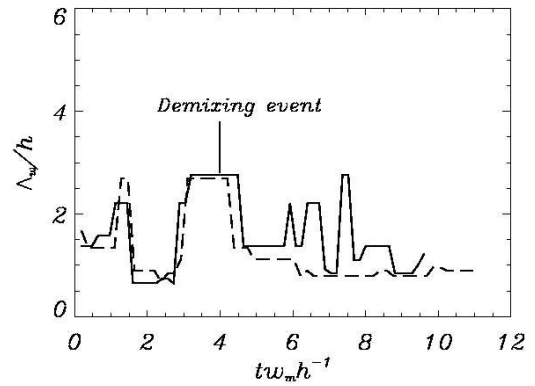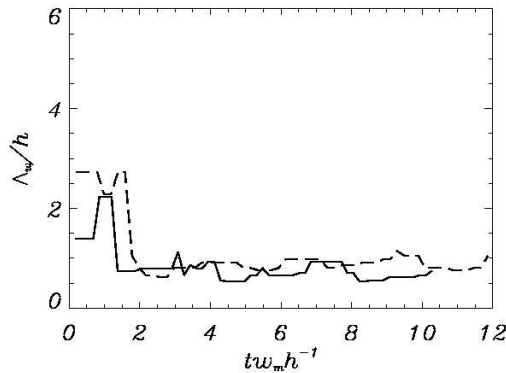

FIGURE 6: Evolution of the spectral peak (characteristic length scale) of the vertical velocity spectra at $z/h \approx 0.5$ as a function of $tw_m h^{-1}$ for NS1 (solid) and NS5 (dashed).

If the evolution of the peak of the horizontal velocity spectra (Λ_u) is considered differences also exist between shear and no shear cases. Figure 8 shows the evolution of Λ_u for the NS cases. For both cases, Λ_u increases its value becoming of the order of the horizontal domain. In order to explain this fact, the evolution of the spectra should be analyzed (not shown here). While the spectral density of the horizontal velocity rapidly decreases for the small scales, the density at large scales remains approximately constant during the decay of convective turbulence. This hints at a form of spectral blockage: spectral transfer is somehow absent or largely reduced at these large scales. As a result, the characteristic length scale moves towards the largest scales. If the horizontal velocity cross section at $z/h \approx 0.5$ is plotted, a unique structure that occupies the whole horizontal domain can be

observed. The shear cases (figure 9) present a similar evolution until $tw_m h^{-1} \approx 4$. The characteristic length scale also increases for GC, however it does not reach the horizontal domain size. In this case, probably due to the continuous shear production there is no spectral blockage at the large scales and the energy decay at the smaller scales does not take place that quickly. The differences obtained at the end of the simulation can be explained by the appearance in both shear cases of two maxima with a similar height at h and $4h$, which makes difficult to determine the characteristic length scale.

FIGURE 7: Evolution of the spectral peak (characteristic length scale) of the vertical velocity spectra at $z/h \approx 0.5$ as a function of $tw_m h^{-1}$ for GC1 (solid) and GC5 (dashed).
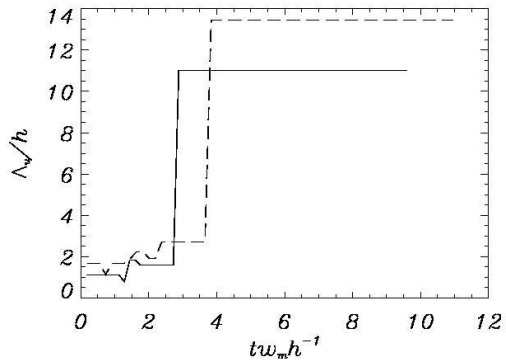

FIGURE 8: Evolution of the spectral peak (characteristic length scale) of the horizontal velocity spectra at $z/h \approx 0.5$ as a function of $tw_m h^{-1}$ for NS1 (solid) and NS5 (dashed).

4. CONCLUSIONS

The influence of the inversion strength and shear during the decay of convective turbulence at sunset over land is studied by means of large eddy simulations. The demixing process discussed previously by NB86 appeared for all the simulated cases, but with different strength which depends on $\Delta\theta$ and on wind shear. We show that weak inversion strengths and shear enhance entrainment favoring the demixing process to occur. For

all the studied cases the spectral peak of the vertical velocity varies during the decay of turbulence. In the cases without shear, the characteristic length scale increases during the demixing events. If demixing is not present, the characteristic length scale is approximately equal to the boundary layer depth with a tendency to decrease for $tw_m h^{-1} > 4$. For the shear cases, the characteristic length scale of the vertical velocity does not change after $tw_m h^{-1} \approx 1$, even when there is a positive buoyancy flux (demixing). This fact, also found by NB86, should be analyzed in more detail by studying the evolution of the bulk values of the terms of the budget equations. We have also shown that the characteristic length scale for the horizontal velocity increases in all the cases.
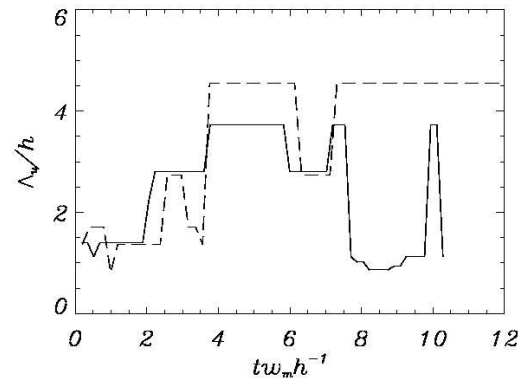

FIGURE 9: Evolution of the spectral peak (characteristic length scale) of the horizontal velocity spectra at $z/h \approx 0.5$ as a function of $tw_m h^{-1}$ for GC1 (solid) and GC5 (dashed).

REFERENCES

Anfossi D., Schayes G., Degrazia G., and A. Goulart, 2004: Atmospheric Turbulence Decay during the Solar Total Eclipse of 11 August 1999. *Bound.-Layer Meteor.*, **111**, 301–311.

Caughey, S. J. and J. C. Kaimal, 1977: Vertical Heat Flux in the Convective Boundary Layer. *Quart. J. Roy. Meteor. Soc.*, **103**, 811–815.

Chasnov, J. R., 1994: Similarity States of Passive Scalar Transport in Isotropic Turbulence. *Phys. Fluids*, **6**, 1036–1051.

Goulart A., Degrazia G., Rizza U., and D. Anfossi, 2003: A Theoretical Model for the Study of Convective

Turbulence Decay and Comparison with Large-Eddy Simulation Data. *Bound.-Layer Meteor.*, **107**, 143–155.

Grant, A. L. M., 1997: An Observational Study of the Evening Transition Boundary Layer. *Quart. J. Roy. Meteor. Soc.*, **123**, 657–677.

Grimsdell, A. W. and W. M. Angevine, 2002: Observations of the Afternoon Transition of the Convective Boundary Layer. *J. Appl. Meteor.*, **41**, 3–11.

Nieuwstadt, F. T. M. and R. A. Brost, 1986: The Decay of Convective Turbulence. *J. Atmos. Sci.*, **43**, 532–546.

Pino, D., Vilà-Guerau de Arellano, J. and P. G. Duynkerke, 2003: Role of the Shear in a Convective Boundary Layer. *J. Atmos. Sci.*, **60**, 1913–1926.

Shaw, W. J. and J. C. Barnard, 2002: Direct Numerical Simulation Decay. In *Proceedings of the 15th Conference on Boundary Layer and Turbulence*, 398–401.

Sorbjan, Z., 1997: Decay of Convective Turbulence Revisited. *Bound.-Layer Meteor.*, **82**, 501–515.

Stillinger , D. C., Helland, K. N. and C. W. Van Atta, 1983: Experiments on the Transition of Homogeneous Turbulence to Internal Waves in a Stratified Fluid. *J. Fluid Mech.* , **131**, 91–122.